Fuel Minimization of the Electric Engine Cooling System With Active Grille Shutter by Iterative Quadratic Programming

Lei Feng, *Member, IEEE*, Jan Wikander, *Member, IEEE*, and Zhiwu Li, *Fellow, IEEE*

***Abstract*—The electric engine cooling system with the active grille shutter requires intelligent and predictive control to reach its full benefits on fuel economy and thermal management. Conventional control methods regulate the coolant temperature to a fixed value but do not directly minimize the vehicle's fuel/energy consumption. By contrast, we design a fuel minimization controller through solving constraint nonlinear optimization problems, whose cost function is the total fuel consumption and constraints are the vehicle's physical limits. To achieve high computational efficiency and sufficient accuracy, the optimization problem is solved by iterative convex quadratic programming and quasilinearization. The advantages of the proposed control method on both fuel economy and engine thermal management are demonstrated by simulations.**

***Index Terms*—Fuel economy, Engine cooling system, Active grille shutter, Quadratic programming, Quasilinearization.**

I. Introduction

THE engine cooling system regulates the temperature of the internal combustion engine and is vital for the engine's thermal safety, performance, fuel economy, emission characteristics, etc. A conventional engine cooling system contains a coolant pump and a radiator fan that are both mechanically coupled to the engine crankshaft through belts, which have little flexibility on the output speed and low energy efficiency. The electric engine cooling system uses electric motors to drive the coolant pump and/or the radiator fan. The higher energy efficiency and better controllability of the electric motors achieve less auxiliary fuel consumption and better engine thermal management [1]–[9]. Another new technology beneficial for both fuel economy and engine thermal management is the active grille/radiator shutter (AGS) [10]–[14]. If the shutter is not fully open, part of the front airflow is blocked from entering the engine compartment and circumvents to sides and undercarriage. Such airflow creates less aerodynamic drag than the same amount of airflow entering the engine compartment and hence reduces fuel consumption. On the thermal aspect, reduced radiator airflow is favorable when the engine temperature is low [15], but detrimental when its temperature is high. Therefore, the shutter control must accommodate the contradictory objectives of reducing aerodynamic drag and improving the cooling system's performance [16]–[18].

Because of the tight coupling of the shutter and the cooling system, the two must be controlled together as an integrated system to reach optimal fuel economy, better thermal management, and the satisfaction of all constraints. Simple feedback controllers using rules and lookup tables are reported in [19]–[22]. These controllers determine the shutter position according to engine oil temperature, coolant temperature, environment temperature, the vehicle speed, etc. While demonstrating the benefits of cooling systems with the active grille shutter, these simple controllers neither directly minimize the total fuel/energy consumption of the vehicle nor explicitly satisfy all constraints.

The predictive [23] and optimal control strategies are more effective for the two objectives. Karnik *et al.* [16] and Bonkoski *et al.* [17] formulate a model predictive controller (MPC) for temperature regulation and constraint satisfaction for advanced cooling systems with a continuous grille shutter, but the method does not directly minimize the energy consumption. By contrast, Cho *et al.* [18] formulate an optimal control approach where the power consumption by the aerodynamic drag is the cost function and the radiator heat rejection rate is the constraint; however, the method neither considers the energy consumption of the cooling actuators nor explicitly enforces the boundary constraint on coolant temperature. Moreover, the optimization is solved by a greedy algorithm that minimizes the power consumption at every step.

To the best of our knowledge, there is no optimal control method for the electric cooling system with the active grille shutter that directly minimizes total fuel consumption, explicitly satisfies all constraints, and exploits the coolant and battery as energy buffers. The smart usage of the battery largely contributes to fuel reduction. When the battery provides electricity to the cooling actuators, the engine has less auxiliary load. When the battery is recharged, the energy may come from either the engine or the vehicle kinetic energy through the regenerative

Manuscript received April 21, 2019; revised September 9, 2019; accepted December 15, 2019. Date of publication January 28, 2020; date of current version March 12, 2020. This work was supported in part by the EU FP7 Project Complete Vehicle Energy-saving Technologies for Heavy-Trucks (CONVENIENT), Project No. 312314, and KTH XPRES, in part by the National Natural Science Foundation of China under Grants 61873342, 61472295, and 61562015, and in part by the Recruitment Program of Global Experts, and the Science and Technology Development Fund, MSAR, under Grant 0012/2019/A1. The review of this article was coordinated by Dr. H. Zhang *(Corresponding author: Lei Feng.)*

L. Feng and J. Wikander are with the Department of Machine Design, KTH Royal Institute of Technology, Stockholm 100 44, Sweden (e-mail: lfeng@kth.se; janwi@kth.se).

Z. Li is with the Institute of Systems Engineering, Macau University of Science and Technology, Macau 999078, China, and also with the School of Electro-Mechanical Engineering, Xidian University, Xi'an 710071, China (e-mail: zhwli@xidian.edu.cn).

Digital Object Identifier 10.1109/TVT.2019.2962866

brake [24]. In the latter case, the generated electricity is free and can significantly reduce the fuel consumption of the electric cooling system. Energy buffers of the electric cooling system are elaborated in Section 1.2 of [9].

The paper has two contributions. One is an optimal control approach that uses the accumulated fuel consumption caused by the cooling actuators and the aerodynamic drag along the entire drive cycle as the cost function and all applicable limits as hard constraints. To achieve high computational efficiency and sufficient accuracy, the original nonlinear cost function is approximated as a convex quadratic function and the non-convex state update model and constraints are approximated as linear time-varying (LTV) models. Then the optimization problem is solved by iterative convex quadratic programming (QP) [25] and quasilinearization [26]. The other is to systematically study the properties of the iterative QP method, including convergence, robustness, optimality, and scalability.

Simulation studies with trucks of different weights on two long and realistic drive cycles show the improved fuel efficiency. Compared to a rule-based baseline controller, the proposed method can reduce the total fuel consumption by 0.39% to 0.70% and the alternator fuel consumption by 32.67% to 58.6%. The reduction on the total consumption appears small, because the percentage of the energy consumption by the cooling system over that by the complete vehicle is less than 1.2%. Compared to the same truck and the same cooling system without the grille shutter, the active shutter can reduce the total fuel consumption by 0.13% to 0.25%. The mean value of the coolant temperature is increased by 5.5 °C to 8.1 °C.

Owing to limited resource, the paper has a few limitations. First, the optimal trajectories of control inputs are computed for the entire drive cycle. Real-time MPC implementation will be developed in future work. Second, the paper investigates only the fuel saving potential by reducing the engine torque through the control of the electric cooling system. The possible benefit of higher coolant temperature, which may increase combustion efficiency in the engine and reduce friction of the lubricant oil [27], is not studied owing to lack of measurement data for the experimental truck. Third, the influence of our controller on tailpipe exhaust emission is not quantitatively studied. We will integrate emission control and fuel reduction control [28]–[30] in the future.

Section II introduces the models of the electronic cooling system with the active grille shutter. Section III formalizes the optimal control problem and proposes an efficient solution based on linear time-varying model approximation and quadratic programming. To improve the accuracy of the solution, Section IV uses quasilinearization to iteratively find better solutions. Section V verifies the advantages of the proposed approach through simulations. Section VI concludes the paper and suggests future works.

II. Models of the Electric Cooling System

The electric cooling system contains a coolant circuit, an electric coolant pump, a number of parallel installed electric radiator fans, a wax-based thermostat, and a shutter, as illustrated in Fig. 1. This section briefly introduces control-oriented models of these components. More details on these models are provided in [9], [13], [14].

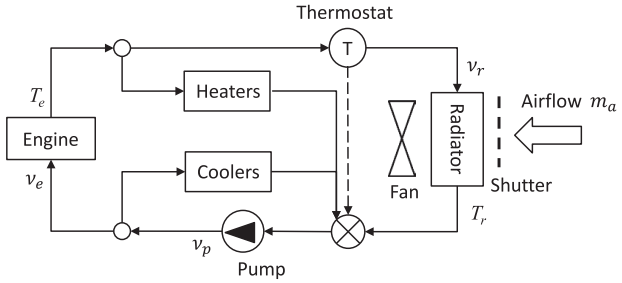

Fig. 1. The Coolant Circuit and Cooling Actuators.

A. Coolant Temperature

The model of the coolant temperature is determined by

$$\dot{T}_e = c_1 Q_{in}(\tau_e, \omega_e) - \frac{\nu_r m_r}{c_2 \nu_r + c_3 m_r}(T_e - T_a) \tag{1}$$

where T_e is coolant temperature at the engine outlet (or coolant temperature for simplicity), T_a the ambient temperature, Q_{in} the heat power transmitted from the engine to the coolant, ν_r coolant volumetric flow rate through the radiator, m_r air mass flow rate through the radiator. Parameters c_1, c_2, and c_3 are constants obtained by model identification. The formula is simplified from those in [7], [31], [32]. The justification, parameter identification and verification of (1) are elaborated in [9].

The radiator coolant volumetric flow rate ν_r is determined by the pump coolant volumetric flow rate ν_p and the thermostat opening ratio $\theta_m \in [0, 1]$. The pump coolant flow rate is determined by its speed ω_p and the thermostat ratio determined by the coolant temperature T_e according to (2).

$$\theta_m(T_e) = \begin{cases} 1 & T_e \geq T_{e1} \\ 0 & T_e \leq T_{e0} \\ \frac{T_e - T_{e0}}{T_{e1} - T_{e0}} & T_{e0} < T_e < T_{e1} \end{cases} \tag{2}$$

In summary, the value of ν_r is determined by T_e and ω_p as follows.

$$\nu_r(T_e, \omega_p) = \theta_m(T_e)\nu_p(\omega_p)$$

The air mass flow rate through the radiator m_r is determined by the shutter position $s \in [0, 1]$, fan speed ω_f, and vehicle speed v. When there is no shutter, the radiator air mass flow rate is a function of ω_f and v, denoted as $m_a(\omega_f, v)$. The shutter decreases the airflow by covering part of the radiator. When the shutter is fully closed ($s = 0$), the ratio between the uncovered radiator area and the total area is $\theta_{s0} < 1$. When the shutter is fully open ($s = 1$), the ratio between the uncovered radiator area and the total area is θ_{s1}. It must be true that $0 \leq \theta_{s0} < \theta_{s1} \leq 1$. For an arbitrary $s \in [0, 1]$, the area-reduction factor is estimated by the linear function

$$\theta_s(s) = \theta_{s0} + (\theta_{s1} - \theta_{s0})s \tag{3}$$

Therefore, the radiator air mass flow rate is estimated as follows.

$$m_r(s, \omega_f, v) = \theta_s(s) m_a(\omega_f, v)$$

The determination of $m_a(\omega_f, v)$ is presented in Section II-C.

B. The Electric Coolant Pump

The models of the electric pump are built from measurement data on the coolant volumetric flow rate and electrical power consumption. The volumetric flow rate is approximately a linear function of the pump speed:

$$\nu_p = \lambda_1 \omega_p + \lambda_0, \tag{4}$$

where ν_p (liter/min) is the coolant volumetric flow rate through the pump, ω_p (rpm) is the pump speed in the range $[\omega_{p\_min}, \omega_{p\_max}]$ and λ_1 and λ_0 are constant coefficients calculated by curve fitting.

The electrical power consumption dependent on the pump speed is approximated as a quadratic function:

$$P_{pmp} = p_2\, \omega_p^2 + p_1\, \omega_p + p_0, \tag{5}$$

where P_{pmp} is the electrical power consumption of the coolant pump and p_2, p_1 and p_0 are constant coefficients calculated by curve fitting [9].

C. The Electric Radiator Fan

The cooling system of the studied truck consists of multiple identical electric fans in parallel. The model here is for the overall effect of all fans. Without the shutter, the total air mass flow rate (in kg/s) through the radiator is a function of fan speed ω_f (rpm) and vehicle speed v (m/s). The function is measured as a 2D lookup table $m_a(\omega_f, v)$ in the region $0 \le \omega_f \le \omega_{f\_max}$, $0 \le v \le v_{max}$. The relation of the electrical power consumption and fan speed is approximately a quadratic function obtained from measurement data.

$$P_{fan} = f_2\, \omega_f^2 + f_1\, \omega_f + f_0, \tag{6}$$

where P_{fan} is the electrical power consumption of the fans, and f_2, f_1, f_0 are constant coefficients [9].

D. The Battery and the Alternator

The alternator converts the mechanical energy of the engine into electricity and is the primary power source for the electrical system. The battery is in parallel connection with the alternator output and serves as an energy buffer. A detailed description of the electrical system is presented in Section 2.5 of [9]. Battery model is a complex research topic. Our prior article [9] adopts a simple battery model based on the measurement data of the studied battery. Although the nominal voltage of the battery is 24 V, the measurement data show that the battery voltage quickly surges to a high value around 29 V during fast charging and slowly declines to a lower value around 25 V during normal operations. Then we simply estimate the battery output voltage U_b by two distinct values depending on whether the regenerative brake is applied, which is determined by the method in Section II-E.

Denote the current through the battery as I_b (A). If I_b is positive/negative, the battery is charged/discharged. Let Q_b be the nominal capacity of the battery's electric charge. Then the change rate of SOC is

$$\dot{SOC} = \frac{\eta_c I_b}{Q_b}, \tag{7}$$

where η_c is the coulombic efficiency of the battery and estimated from the measurement data. Its value is typically 1 when discharging and less than 1 when charging. The output power of the battery is

$$P_{bat} = U_b I_b. \tag{8}$$

The alternator electrical power P_{alt} is calculated as

$$P_{alt} = P_{pmp} + P_{fan} + P_{bat} + P_{oth},$$

where P_{oth} is additional power consumption of other electrical loads including lights and ECUs. By (5), (6) and (8), the alternator electrical power is a quadratic function of ω_p, ω_f, and I_b,

$$P_{alt} = [\omega_p, \omega_f, I_b] \begin{bmatrix} p_2 & 0 & 0 \\ 0 & f_2 & 0 \\ 0 & 0 & 0 \end{bmatrix} \begin{bmatrix} \omega_p \\ \omega_f \\ I_b \end{bmatrix} + \begin{bmatrix} p_1 \\ f_1 \\ U_b \end{bmatrix}^T \begin{bmatrix} \omega_p \\ \omega_f \\ I_b \end{bmatrix} + p_0 + f_0 + P_{oth}$$

The alternator current I_{alt} is $I_{alt} = \frac{P_{alt}}{U_b}$. The maximal current supply of the alternator is a function of the engine speed and the alternator current cannot be negative. Therefore

$$0 \le I_{alt} \le I_{alt\_max}(\omega_e) \tag{9}$$

The alternator is connected to the engine's crankshaft via belts and adds additional torque to the engine crankshaft. The alternator's average power efficiency is dependent on engine speed, denoted as $\eta_a(\omega_e)$. Owing to the friction of the alternator and the belt transmission, we consider a minimal mechanical power loss of the alternator, denoted as $M_{alt}(\omega_e)$. Finally the alternator's additional torque on the engine crankshaft is

$$\tau_a = \frac{1}{\omega_e} \max\left(M_{alt}(\omega_e), \frac{P_{alt}}{\eta_a(\omega_e)} \right). \tag{10}$$

For the purpose of reducing fuel consumption, there is no benefit to have P_{alt} less than $M_{alt}(\omega_e)\eta_a(\omega_e)$. Therefore we replace (10) by an equation and an inequality:

$$\tau_a = \frac{P_{alt}}{\omega_e\, \eta_a(\omega_e)} \tag{11}$$

$$M_{alt}(\omega_e)\eta_a(\omega_e) \le P_{alt} \tag{12}$$

The combination of (9) and (12) is equal to the constraint

$$M_{alt}(\omega_e)\eta_a(\omega_e) \le P_{alt} \le I_{alt\_max}(\omega_e) U_b.$$

By (11) we have a further constraint on the alternator torque

$$\tau_{a\_min}(\omega_e) \le \tau_a \le \tau_{a\_max}(\omega_e) \tag{13}$$

where

$$\tau_{a\_min}(\omega_e) = \frac{M_{alt}(\omega_e)}{\omega_e}, \tau_{a\_max}(\omega_e) = \frac{I_{alt\_max}(\omega_e)U_b}{\omega_e\,\eta_a(\omega_e)}$$

E. Driveline Torque

The engine's crankshaft is connected to the gearbox through a clutch. The torque applied at the input shaft of the gearbox is the driveline torque τ_d. Assume that all relevant vehicle parameters and the drive cycle are known, including the trajectories of speed and slope angle. Under the common assumption that all vehicle components are stiff and the tire slip ratio is zero, the traction force F_t between the driving wheels and the ground can be computed by the standard approach [33], [34]. The aerodynamic drag $F_a(v, s)$ is a term of F_t and dependent on both vehicle speed and the shutter position.

$$F_a(v, s) = \frac{1}{2}\rho_a A_f c_d(s) v^2 \tag{14}$$

where ρ_a is the air density, A_f the front area, v the speed in m/s, and $c_d(s)$ the drag coefficient dependent on the shutter position s. Through wind-tunnel experiments we find the coefficient values c_{d0} and c_{d1} corresponding to completely closed and open shutter, respectively. For an arbitrary opening ratio $s \in [0, 1]$ the drag coefficient is estimated as

$$c_d(s) = c_{d0} + (c_{d1} - c_{d0})\, s \tag{15}$$

The traction force F_t is realized by the driveline torque τ_d and the brake torque τ_b through the transmission. Let n be the gear number, $i_t(n)$ the total transmission ratio including both the gearbox and the final gear, $\eta_t(n)$ the total transmission efficiency, and r_w the radius of the driving wheels.

$$F_t = \begin{cases} \dfrac{1}{r_w}\left[i_t(n)\eta_t(n)\tau_d - \tau_b\right], & \tau_d \geq 0 \\ \dfrac{1}{r_w}\left[\dfrac{i_t(n)}{\eta_t(n)}\tau_d - \tau_b\right], & \tau_d < 0 \end{cases} \tag{16}$$

F. The Engine Model

The engine is characterized by the fuel rate map and the heat release map from measurement. Both are 2D lookup tables dependent on the engine's torque and speed. The engine fuel rate map $\dot{m}_f$ is approximated by a quadratic function of the engine torque at different engine speeds, i.e.,

$$\dot{m}_f(\tau_e, \omega_e) = r_2(\omega_e){\tau_e}^2 + r_1(\omega_e)\tau_e + r_0(\omega_e). \tag{17}$$

The map of heat transfer to the coolant is approximated by linear functions at different engine speeds.

$$\dot{Q}_{in}(\tau_e, \omega_e) = h_1(\omega_e)\tau_e + h_0(\omega_e). \tag{18}$$

The speed-dependent coefficients in (17) and (18) are obtained by curve-fitting methods elaborated in [9].

The engine speed is calculated from the vehicle speed and the transmission ratio.

$$\omega_e = \frac{v}{r_w} i_t(n)$$

The torque value τ_e is the effective torque at the engine crankshaft. Owing to internal friction, τ_e may be negative. The minimal engine torque $\tau_{e\_min} < 0$ is equivalent to the internal friction torque at which the engine fuel rate is 0, and the value is dependent on the engine speed.

The effective engine torque is equal to the sum of the driveline torque and alternator torque.

$$\tau_e = \tau_d(s) + \tau_a \tag{19}$$

where τ_a is calculated from the three control variables ω_p, ω_f, I_b via (10) and always positive. When $\tau_d(s) \geq 0$, the engine provides torque to both the driveline and the alternator. When $\tau_d(s) < 0$, the driveline requires brake torque at the input shaft of the gearbox. When the negative driveline torque is within the range $\tau_d(s) + \tau_a \geq \tau_{e\_min}$, the brake torque is fulfilled by the combination of engine friction and alternator load. This suggests that vehicle brake torque may drive the alternator for generating electricity, enabling regenerative brake for energy recovery. When the negative driveline torque $\tau_d(s)$ is so small that $\tau_d(s) + \tau_a < \tau_{e\_min}$, the friction brakes at the wheels must be engaged. On the other hand, the sum of the driveline torque and the alternator torque cannot exceed the maximal engine torque: $\tau_d(s) + \tau_a \leq \tau_{e\_max}$. The inequality yields a new constraint on τ_a: $\tau_a \leq \tau_{e\_max} - \tau_d(s)$. Denote $\tau_{d0} = \tau_d(0)$ and $\tau_{d1} = \tau_d(1)$. Since $\tau_{d0} \leq \tau_d(s) \leq \tau_{d1}$, $\tau_{e\_max} - \tau_{d1} \leq \tau_{e\_max} - \tau_d(s)$ for all $s \in [0, 1]$. The inequality above is replaced by the following stronger constraint.

$$\tau_a \leq \tau_{e\_max} - \tau_{d1}$$

The alternator torque is also bounded by its own physical limit as in (13). The two inequalities both constrain the upper bound of the alternator torque. Denote the actual upper bound of the alternator torque as

$$\tau_{a\_ub} = \begin{cases} \tau_{a\_max}, & \tau_{e\_max} - \tau_{d1} \geq \tau_{a\_max} \\ \tau_{e\_max} - \tau_{d1}, & \tau_{a\_max} > \tau_{e\_max} - \tau_{d1} \geq \tau_{a\_min} \\ \tau_{a\_min}, & \tau_{a\_min} > \tau_{e\_max} - \tau_{d1} \end{cases}$$

Then the constraint of (13) on the alternator torque becomes

$$\tau_{a\_min} \leq \tau_a \leq \tau_{a\_ub}$$

III. The Optimal Control Problem

The control objective is to minimize the total fuel consumption for a given drive cycle, which contains timed signals of vehicle speed $v(t)$ and road slope angle $\theta(t)$, where $0 \leq t \leq T$ and T is the traveling time of the drive cycle. This paper assumes that the truck follows the driving cycle without any deviation. Let Δt be the sampling time and N the length of the drive cycle, i.e., $T = N\Delta t$. The discrete-time state space model of the electric cooling system and the battery is the following:

$$\begin{bmatrix} T_e(k+1) \\ SOC(k+1) \end{bmatrix} = \begin{bmatrix} T_e(k) + \dot{T}_e(k)\Delta t \\ SOC(k) + \frac{\eta_c I_b(k)}{Q_b}\Delta t \end{bmatrix} \tag{20}$$

where $k = 0, 1, \ldots, N-1$ and $\dot{T}_e(k)$ is calculated by (1) at time $k\Delta t$. Let the state vector be $\mathbf{x}(k) = [T_e(k), SOC(k)]^T$, the control input vector $\mathbf{u}(k) = [\omega_p(k), \omega_f(k), I_b(k), s(k)]^T$,

and the disturbance vector $\mathbf{w}(k) = [\dot{v}(k), v(k), n(k), \theta(k)]^T$. Eq. (20) is simply denoted by

$$\mathbf{x}(k+1) = \mathbf{f}\left(\mathbf{x}(k), \mathbf{u}(k), \mathbf{w}(k)\right)$$

The optimal control problem is formalized as follows.

$$\min_{\mathbf{u}(0),\ldots,\mathbf{u}(N-1)} \sum_{k=0}^{N-1} \dot{m}_f\left[\tau_e\left(\mathbf{u}(k), \mathbf{w}(k)\right), \omega_e(k)\right] \tag{21a}$$

subjec to (20) and the following constraints

$$SOC(0) - \epsilon \le SOC(N) \le SOC(0) + \epsilon \tag{21b}$$

$$T_{e\_min} \le T_e(k) \le T_{e\_max} \tag{21c}$$

$$SOC_{min} \le SOC(k) \le SOC_{max} \tag{21d}$$

$$\omega_{p\_min} \le \omega_p(k) \le \omega_{p\_max} \tag{21e}$$

$$0 \le \omega_f(k) \le \omega_{f\_max} \tag{21f}$$

$$I_{b\_min} \le I_b(k) \le I_{b\_max} \tag{21g}$$

$$0 \le s(k) \le 1 \tag{21h}$$

$$\tau_{a\_min}(k) \le \tau_a(k) \le \tau_{a\_ub}(k) \tag{21i}$$

In (21b), ϵ is a small positive number. The problem is solvable by offline global optimal control methods including dynamic programming (DP) [35]–[37] and Pontryagin's minimum principle (PMP) [24], [38], [39]. Since the offline methods rely on accurate dynamic model and the full knowledge of the drive cycle, and are expensive in computation time and memory consumption, they are not suitable for real-time feedback control with embedded microprocessors. In the following, we simplify the problem to benefit from more efficient optimization solvers.

The objective in (21a) is to minimize the total fuel consumption for both vehicle traction and auxiliaries. Given the assumption that the vehicle exactly follows the drive cycle and the torque demand of the auxiliaries does not alter gear selection, the fuel consumption for vehicle traction is invariant of the control demands of the cooling system, i.e., pump speed, fan speed, and battery current. Furthermore the default position of the shutter is open. Decreasing its opening position only slightly decreases the driveline torque. Consequently the objective function can be changed to the fuel consumption variation caused by the cooling system and the shutter.

Let $\Delta\dot{m}_f(k)$ be the fuel rate variation at time $k\Delta t$. For simplicity we skip the argument k in the following discussion.

$$\Delta\dot{m}_f = \dot{m}_f\left(\tau_d(s) + \tau_a,\ \omega_e\right) - \dot{m}_f\left(\tau_{d1} + \tau_{a\_min},\ \omega_e\right)$$

where $\tau_{a\_min} \le \tau_a \le \tau_{a\_ub}$ and τ_{d1} is the driveline torque when $s = 1$. Because $\tau_a \ll |\tau_{d1}|$ and $|\tau_d(s) - \tau_{d1}| \ll |\tau_{d1}|$, $\Delta\dot{m}_f$ is estimated as follows according to the quadratic engine fuel rate model in (17).

$$\Delta\dot{m}_f \approx \alpha_f(\tau_a - \tau_{a\_min}) + \alpha_f(\tau_d(s) - \tau_{d1}) \tag{22}$$

where $\alpha_f = 2r_2(\omega_e)(\tau_{d1} + \tau_{a\_min}) + r_1(\omega_e)$ is the derivative of fuel rate over engine torque. Its value is independent of the control input. If $\tau_{d1} + \tau_{a\_max} \le \tau_{e\_min}$, the brake torque from the driveline can produce the maximal alternator torque and still keep the engine fuel rate to be zero. All energy to drive the cooling system and charge the battery comes from the kinetic energy and hence does not consume any fuel. α_f is then refined as

$$\alpha_f = \begin{cases} 0, \ \tau_{d1} + \tau_{a\_max} \le \tau_{e\_min} \\ 2r_2(\omega_e)(\tau_{d1} + \tau_{a\_min}) + r_1(\omega_e), \text{otherwise} \end{cases}$$

$\Delta\dot{m}_f$ is linear in the driveline torque $\tau_d(s)$ and the alternator torque τ_a. The first term of (22) is identical to our previous result on estimating the fuel consumption of the cooling system [9]. The second term of (22) estimates the fuel consumption reduction owing to the reduced aerodynamic drag.

According to Section II-D, τ_a is the quadratic function

$$\begin{aligned}\tau_a = \frac{P_{alt}}{\omega_e\eta_a(\omega_e)} = \frac{1}{\omega_e\eta_a(\omega_e)}\left(p_2\omega_p^2 + f_2\omega_f^2\right. \\ \left. + p_1\omega_p + f_1\omega_f + U_bI_b + p_0 + f_0 + P_{oth}\right)\end{aligned} \tag{23}$$

In the expression of $\alpha_f(\tau_a - \tau_{a\_min})$, p_0, f_0, P_{oth}, and τ_{a_min} are irrelevant of the control input $\mathbf{u}$. We then remove them and simplify the first term of $\Delta\dot{m}_f$ to a quadratic cost function.

$$cost_1 := \alpha\left(\mathbf{u}^T\begin{bmatrix} p_2 & 0 & 0 & 0 \\ 0 & f_2 & 0 & 0 \\ 0 & 0 & 0 & 0 \\ 0 & 0 & 0 & 0 \end{bmatrix}\mathbf{u} + \begin{bmatrix} p_1 \\ f_1 \\ U_b \\ 0 \end{bmatrix}^T\mathbf{u}\right)$$

where

$$\alpha = \frac{\alpha_f}{\omega_e\eta_a(\omega_e)} \tag{24}$$

Note that α is dependent on the driveline torque and the engine speed, and hence a function of time. Ignoring the brake torque τ_b in (16), we calculate the driveline torque demand $\tau_d(s)$ as follows.

$$\tau_d(s) = F_t(s)\beta_t \tag{25}$$

where

$$\beta_t = \begin{cases} \dfrac{r_w}{i_t(n)\eta_t(n)}, & F_t(s) \ge 0 \\ \dfrac{r_w\eta_t(n)}{i_t(n)}, & F_t(s) < 0 \end{cases}$$

is the conversion ratio from the traction force at the wheels to the torque at the gearbox input. The equation shows the dependency of β_t on the control input s. For example, it is possible that when $s = 1$, $F_t(1) \ge 0$ but when $s = 0$, $F_t(0) < 0$. The switching possibility complicates the calculation of $\tau_d(s)$ and prevents us from solving this optimization problem by QP. In quantity, the difference between $F_t(1)$ and $F_t(0)$ is very small. We can simply replace $F_t(s)$ by $F_t(1)$ (or $F_t(0)$) to evaluate β_t, i.e.,

$$\beta_t = \begin{cases} \dfrac{r_w}{i_t(n)\eta_t(n)}, & F_t(1) \ge 0 \\ \dfrac{r_w\eta_t(n)}{i_t(n)}, & F_t(1) < 0 \end{cases} \tag{26}$$

To obtain $F_t(s)$, only $F_a(v,s)$ is related to the control input s by (14). The derivative of $F_t(s)$ over s is

$$\beta_a := \frac{d\,F_t(s)}{d\,s} = \frac{1}{2}\rho_a A_f\,(c_{d1} - c_{d0})\,v^2 \tag{27}$$

Ignoring parameters irrelevant of the control input, we have the cost function of the second term of (22) as

$$cost_2 := [0,0,0,\beta]\,\mathbf{u}$$

where $\beta = \alpha_f\beta_t\beta_a$. Note that β is dependent on the driveline torque, engine speed, gear number, and vehicle speed. It is hence a function of time. The total cost function is then

$$\begin{aligned} cost &= cost_1 + cost_2 \\ &= \alpha\mathbf{u}^T \begin{bmatrix} p_2 & 0 & 0 & 0 \\ 0 & f_2 & 0 & 0 \\ 0 & 0 & 0 & 0 \\ 0 & 0 & 0 & 0 \end{bmatrix} \mathbf{u} + \begin{bmatrix} \alpha p_1 \\ \alpha f_1 \\ \alpha U_b \\ \beta \end{bmatrix}^T \mathbf{u} \end{aligned}$$

At step k, define

$$H_k := 2\alpha(k) \begin{bmatrix} p_2 & 0 & 0 & 0 \\ 0 & f_2 & 0 & 0 \\ 0 & 0 & 0 & 0 \\ 0 & 0 & 0 & 0 \end{bmatrix}, \mathbf{g}_k := \begin{bmatrix} \alpha(k)p_1 \\ \alpha(k)f_1 \\ \alpha(k)U_b(k) \\ \beta(k) \end{bmatrix} \tag{28}$$

Then the cost function at step $k \in \{0,1,\ldots,N-1\}$ becomes

$$cost(k) = \frac{1}{2}\mathbf{u}^T(k)H_k\mathbf{u}(k) + \mathbf{g}_k^T\mathbf{u}(k)$$

Finally the optimal control problem is reduced to the new quadratic format.

$$\min_{\mathbf{u}(0),\ldots,\mathbf{u}(N-1)} \sum_{k=0}^{N-1} cost(k) \tag{29}$$

subject to the state update equation in (20) and all constraints in (21b)–(21i). Its solution is presented in the next section.

IV. Iterative QP Based on Quasilinearization

The optimal control problem in (29) cannot yet be solved by a QP solver because the state update function in (20) and the constraint in (21i) are nonlinear. This section presents a quasilinearization method [35] to approximate the nonlinear equations by a sequence of linear equations and solve each linear approximation by QP.

A. Linear Time-Varying Model

The nonlinear discrete-time state space model is presented in (20). A fundamental assumption in this work is that the control on the electric cooling system and the radiator shutter does not alter the vehicle speed trajectory and the vehicle exactly follows the drive cycle. This means that the trajectory of the disturbance vectors $\mathbf{w}(k)$ $(k = 0,\ldots,N-1)$ is deterministic for the entire drive cycle. We first linearize the nonlinear model at an arbitrary point $\hat{\mathbf{p}} = (\hat{\mathbf{x}},\hat{\mathbf{u}},\hat{\mathbf{w}})$.

$$\begin{aligned} \mathbf{f}(\mathbf{x},\mathbf{u},\mathbf{w}) \approx{}& \mathbf{f}(\hat{\mathbf{x}},\hat{\mathbf{u}},\hat{\mathbf{w}}) + A_{\hat{\mathbf{p}}}(\mathbf{x}-\hat{\mathbf{x}}) + B_{\hat{\mathbf{p}}}(\mathbf{u}-\hat{\mathbf{u}}) \\ &+ G_{\hat{\mathbf{p}}}(\mathbf{w}-\hat{\mathbf{w}}) \end{aligned}$$

Since it always holds that $\mathbf{w} = \hat{\mathbf{w}}$, the last term is eliminated.

$$\mathbf{f}(\mathbf{x},\mathbf{u},\mathbf{w}) \approx \mathbf{f}(\hat{\mathbf{x}},\hat{\mathbf{u}},\hat{\mathbf{w}}) + A_{\hat{\mathbf{p}}}(\mathbf{x}-\hat{\mathbf{x}}) + B_{\hat{\mathbf{p}}}(\mathbf{u}-\hat{\mathbf{u}}) \tag{30}$$

For simple notation, we write $\hat{\theta}_m$ for $\theta_m(\hat{T}_e)$, $\hat{\nu}_p$ for $\nu_p(\hat{\omega}_p)$, $\hat{\theta}_s$ for $\theta_s(\hat{s})$ and $\hat{m}_a$ for $m_a(\hat{\omega}_f,\hat{v})$. Accordingly, $\hat{\nu}_r = \hat{\theta}_m\hat{\nu}_p$ and $\hat{m}_r = \hat{\theta}_s\hat{m}_a$. To concisely describe the Jacobian matrices we define the variable $\hat{\psi} = c_2\hat{\nu}_r + c_3\hat{m}_r$. The Jacobian matrices in (30) are

$$A_{\hat{\mathbf{p}}} = \begin{bmatrix} 1 - \left(\dfrac{\hat{\nu}_r\hat{m}_r}{\hat{\psi}} + \dfrac{c_3\hat{\dot{\theta}}_m\hat{\nu}_p\hat{m}_r^2}{\hat{\psi}^2}(\hat{T}_e - T_a)\right)\Delta t & 0 \\ 0 & 1 \end{bmatrix} \tag{31a}$$

$$B_{\hat{\mathbf{p}}} = \frac{\partial\mathbf{f}}{\partial\mathbf{u}}|_{\hat{\mathbf{p}}} \tag{31b}$$

The matrix $B_{\hat{\mathbf{p}}}$ is 2×4 and has the following elements

$$B_{\hat{\mathbf{p}}}(1,1) = \left(c_1\frac{\partial Q_{in}}{\partial\tau_e}\frac{\partial\tau_a}{\partial\omega_p}|_{\hat{\mathbf{p}}} - \frac{c_3\hat{\theta}_m\lambda_1\hat{m}_r^2}{\hat{\psi}^2}\left(\hat{T}_e - T_a\right)\right)\Delta t$$

$$B_{\hat{\mathbf{p}}}(1,2) = \left(c_1\frac{\partial Q_{in}}{\partial\tau_e}\frac{\partial\tau_a}{\partial\omega_f}|_{\hat{\mathbf{p}}} - \frac{c_2\hat{\nu}_r^2\hat{\theta}_s}{\hat{\psi}^2}\frac{\partial m_a}{\partial\omega_f}|_{\hat{\mathbf{p}}}\left(\hat{T}_e - T_a\right)\right)\Delta t$$

$$B_{\hat{\mathbf{p}}}(1,3) = c_1\frac{\partial Q_{in}}{\partial\tau_e}\frac{\partial\tau_a}{\partial I_b}|_{\hat{\mathbf{p}}}\Delta t$$

$$B_{\hat{\mathbf{p}}}(1,4) = \left(c_1\frac{\partial Q_{in}}{\partial\tau_e}\frac{\partial\tau_d}{\partial s}|_{\hat{\mathbf{p}}} - \frac{c_2\hat{\nu}_r^2\Delta\theta_s\hat{m}_a}{\hat{\psi}^2}\left(\hat{T}_e - T_a\right)\right)\Delta t$$

$$B_{\hat{\mathbf{p}}}(2,3) = \frac{\eta_c}{Q_b}\Delta t$$

$$B_{\hat{\mathbf{p}}}(2,1) = B_{\hat{\mathbf{p}}}(2,2) = B_{\hat{\mathbf{p}}}(2,4) = 0$$

In $B_{\hat{\mathbf{p}}}(1,4)$, $\Delta\theta_s = \theta_{s1} - \theta_{s0}$. The driveline torque $\tau_d(s)$ is calculated by (25). Then $\partial\tau_d/\partial s = \beta_t\beta_a$ in $B_{\hat{\mathbf{p}}}(1,4)$. By (2), the thermostat opening ratio θ_m is dependent on the coolant temperature. So is the expression of $A_{\hat{\mathbf{p}}}(1,1)$.

$$A_{\hat{\mathbf{p}}}(1,1) = \begin{cases} 1 - \dfrac{\hat{\nu}_p\hat{m}_r}{\hat{\psi}}\Delta t, & \hat{T}_e \geq T_{e1} \\ 1, & \hat{T}_e \leq T_{e0} \\ 1 - \left(\dfrac{\hat{\nu}_r\hat{m}_r}{\hat{\psi}} + \dfrac{c_3\hat{\nu}_p\hat{m}_r^2}{\hat{\psi}^2}\dfrac{\hat{T}_e - T_a}{T_{e1} - T_{e0}}\right)\Delta t, & \text{otherwise} \end{cases}$$

Let $\{\hat{\mathbf{u}}_k | k = 0,1,\ldots,N-1\}$ be a trajectory of estimated control inputs. The trajectory of estimated states is estimated as follows. Let $\hat{\mathbf{x}}_0 = \mathbf{x}(0)$.

$$\hat{\mathbf{x}}_{k+1} = \mathbf{f}(\hat{\mathbf{x}}_k,\hat{\mathbf{u}}_k,\mathbf{w}(k)),\, k = 0,1,\ldots,N-1$$

In real executions, the actual trajectory of control inputs $\{\mathbf{u}(k)|k=0,1,\ldots,N-1\}$ often deviates from the prediction trajectory. Consequently the actual trajectory of states $\{\mathbf{x}(k)|k=0,1,\ldots,N\}$ is also different from the prediction trajectory of states. The relationship of the actual trajectories of states and inputs is approximately the following. For $k=0,1,\ldots,N-1$

$$\mathbf{x}(k+1)=\hat{\mathbf{x}}_{k+1}+A_k\left(\mathbf{x}(k)-\hat{\mathbf{x}}_k\right)+B_k\left(\mathbf{u}(k)-\hat{\mathbf{u}}_k\right) \quad (32)$$

In this equation, A_k and B_k are simple representations of matrices $A_{(\hat{\mathbf{x}}_k,\hat{\mathbf{u}}_k,\mathbf{w}_k)}$ and $B_{(\hat{\mathbf{x}}_k,\hat{\mathbf{u}}_k,\mathbf{w}_k)}$ as defined in (31).

B. Boundary Constraints on Torque

To use standard QP solvers, all constraints must be linear. The constraints below (21a) are all simple boundary constraints on state and control input, except the inequality constraint (21i) on alternator torque. This is because $\tau_a(k)$ is unfortunately quadratic in the control input by (23). Consequently, $\tau_a(k)$ is linearized at the estimated control vector $\hat{\mathbf{u}}_k$.

$$\begin{aligned}\tau_a(k)&\approx\hat{\tau}_a(k)+\left(\frac{\partial\tau_a}{\partial\mathbf{u}}|_{\hat{\mathbf{u}}_k}\right)^T\left(\mathbf{u}(k)-\hat{\mathbf{u}}_k\right)\\&=\frac{1}{\omega_e\eta_a(\omega_e)}\left[\hat{\mathbf{p}}_k^T\mathbf{u}(k)+\Delta\hat{P}_{alt}(k)\right]\end{aligned}$$

where $\hat{\mathbf{p}}_k^T=[2p_2\hat{\omega}_p(k)+p_1,2f_2\hat{\omega}_f(k)+f_1,\hat{U}_b(k),0]$ and $\Delta\hat{P}_{alt}(k)=\hat{P}_{alt}(k)-\hat{\mathbf{p}}_k^T\hat{\mathbf{u}}_k$. This is a linear function of the control input $\mathbf{u}(k)$. Hence the inequality constraint on the alternator torque in (21i) becomes

$$\begin{aligned}\omega_e(k)\eta_a(k)\tau_{a\_min}(k)-\Delta\hat{P}_{alt}(k)&\le\hat{\mathbf{p}}_k^T\mathbf{u}(k)\\&\le\omega_e(k)\eta_a(k)\tau_{a\_ub}(k)-\Delta\hat{P}_{alt}(k)\end{aligned} \quad (33)$$

C. Solution by Quadratic Programming

The objective function of (29) is a quadratic function of the sequence of control inputs. We formalize it as a QP problem and solve it by a QP solver. All unknown variables are organized into the vector

$$\mathbf{z}:=\left[\mathbf{u}^T(0),\ldots,\mathbf{x}^T(k),\mathbf{u}^T(k),\ldots,\mathbf{x}^T(N)\right]^T \quad (34)$$

where $k=1,\ldots,N-1$. Its length is $6\,N$. The total cost becomes a quadratic function of the vector $\mathbf{z}$.

$$\sum_{k=0}^{N-1}\left(\frac{1}{2}\mathbf{u}^T(k)H_k\mathbf{u}(k)+\mathbf{g}_k^T\mathbf{u}(k)\right)=\frac{1}{2}\mathbf{z}^TH\mathbf{z}+\mathbf{g}^T\mathbf{z} \quad (35)$$

where H is a $6\,N\times6\,N$ square matrix such that for $k=0,\ldots,N-1$, $H(6k+1:6k+4,6k+1:6k+4)=H_k$ and other elements are 0. The vector $\mathbf{g}$ is a $6\,N$ vector such that $\mathbf{g}(6k+1:6k+4)=\mathbf{g}_k$ and other elements are 0. Recall that H_k and $\mathbf{g}_k$ are defined in (28).

The linear state update function of (32) is also reformulated as the matrix format.

$$A_{eq}\mathbf{z}=\mathbf{b}_{eq} \quad (36)$$

where A_{eq} is a $2\,N\times6\,N$ matrix and $\mathbf{b}_{eq}$ is a $2\,N$ vector. Their elements are given below. I_2 denotes the 2×2 identity matrix.

For $k=1,\ldots,N-1$,

$$\begin{aligned}A_{eq}(1:2,1:6)&=[-B_0,I_2],\\A_{eq}\left(2k+1:2k+2,6k-1:6k+6\right)&=[-A_k,-B_k,I_2]\\A_{eq}(r,s)&=0,\ \text{otherwise}\end{aligned}$$

and

$$\begin{aligned}\mathbf{b}_{eq}(1:2)&=\hat{\mathbf{x}}_1-B_0\hat{\mathbf{u}}_0\\\mathbf{b}_{eq}(2k+1:2k+2)&=\hat{\mathbf{x}}_{k+1}-A_k\hat{\mathbf{x}}_k-B_k\hat{\mathbf{u}}_k\end{aligned}$$

For $k=0,\ldots,N-1$, all linear inequality constraints in (33) are summarized by a matrix inequality.

$$A_{in}\mathbf{z}\le\mathbf{b}_{in} \quad (37)$$

where A_{in} is a $2N\times6\,N$ matrix and $\mathbf{b}_{in}$ is a $2\,N$ vector.

$$\begin{aligned}A_{in}(2k+1:2k+2,6k+1:6k+4)&=\begin{bmatrix}-\hat{\mathbf{p}}_k^T\\\hat{\mathbf{p}}_k^T\end{bmatrix}\\A_{in}(r,s)&=0,\ \text{otherwise}\end{aligned}$$

$$\mathbf{b}_{in}(2k+1:2k+2)=\begin{bmatrix}-\omega_e(k)\eta_a(k)\tau_{a\_min}(k)+\Delta\hat{P}_{alt}(k)\\\omega_e(k)\eta_a(k)\tau_{a\_ub}(k)-\Delta\hat{P}_{alt}(k)\end{bmatrix}$$

All boundary constraints in (21b)-(21h) are formalized as boundary vectors of $\mathbf{z}$. The lower and upper bound vectors of $\mathbf{z}$ are $\mathbf{L}_b$ and $\mathbf{U}_b$, respectively. They are both $6\,N$ vectors. For $k=0,\ldots,N-1$

$$\begin{aligned}&\mathbf{L}_b(6k+1)=\omega_{p\_min},\ \mathbf{U}_b(6k+1)=\omega_{p\_max}\\&\mathbf{L}_b(6k+2)=0,\ \mathbf{U}_b(6k+2)=\omega_{f\_max}\\&\mathbf{L}_b(6k+3)=I_{b\_min},\ \mathbf{U}_b(6k+3)=I_{b\_max}\\&\mathbf{L}_b(6k+4)=0,\ \mathbf{U}_b(6k+4)=1\\&\mathbf{L}_b(6k+5)=T_{e\_min},\ \mathbf{U}_b(6k+5)=T_{e\_max}\\&\mathbf{L}_b(6k+6)=SOC_{min},\ \mathbf{U}_b(6k+6)=SOC_{max}\\&\mathbf{L}_b(6\,N)=SOC(0)-\epsilon,\ \mathbf{U}_b(6\,N)=SOC(0)+\epsilon\end{aligned}$$

Finally the optimization problem in (29) is formalized as a QP problem of vector $\mathbf{z}$.

$$\min_{\mathbf{z}\in\mathbb{R}^{6\,N}}\frac{1}{2}\mathbf{z}^TH\mathbf{z}+\mathbf{g}^T\mathbf{z}$$

subject to (36), (37), and $\mathbf{L}_b\le\mathbf{z}\le\mathbf{U}_b$. This is a typical QP problem with linear constraints. Since the Hessian matrix H is diagonal and all diagonal elements are non-negative, the Hessian matrix is positive semi-definite. The QP problem is hence convex and can be efficiently solved by the interior point method. This paper solves the QP problem by the `quadprog` function from MATLAB Optimization Toolbox and chooses the `interior-point-convex` algorithm.

D. The Quasilinearization Algorithm

Owing to linearization, the QP solution to (29) is dependent on the estimated trajectories of control inputs $\{\hat{\mathbf{u}}_k|k=0,\ldots,$

Algorithm 1: Quasilinearization Algorithm.

Data: The initial state $\mathbf{x}(0)$ and an estimated sequence of control inputs $\{\hat{\mathbf{u}}_k\}$

Result: The sequences of optimal control inputs and the corresponding state vectors $\{\mathbf{u}^*(k), \mathbf{x}^*(k)\}$ and the minimal fuel consumption fc^*

1 Assign $l^* = 0$;
2 Initiate $\{\mathbf{u}_k^{(0)} = \hat{\mathbf{u}}_k\}$;
3 Compute $\{\mathbf{x}_k^{(0)}\}$ by (20), $\mathbf{x}(0)$, and $\{\mathbf{u}_k^{(0)}\}$;
4 Compute fuel consumption $fc^{(0)}$ by (21a) and $\{\mathbf{u}_k^{(0)}\}$;
5 **for** $l = 1$ **to** $maxIter$ **do**
6 Formulate a QP problem using $\{\mathbf{u}_k^{(l-1)}, \mathbf{x}_k^{(l-1)}\}$ according to Section IV-C;
7 Obtain the optimal control and linear state sequences $\{\mathbf{u}_k^{(l)}, \overline{\mathbf{x}}_k^{(l)}\}$ by solving the QP problem;
8 Compute $\{\mathbf{x}_k^{(l)}\}$ by (20), $\mathbf{x}(0)$, and $\{\mathbf{u}_k^{(l)}\}$;
9 Compute fuel consumption $fc^{(l)}$ by (21a) and $\{\mathbf{u}_k^{(l)}\}$;
10 Compute $d_i = \sqrt{\frac{\sum_{k=1}^{N}(\mathbf{x}_k^{(l)}(i) - \overline{\mathbf{x}}_k^{(l)}(i))^2}{N}}$ for $i = 1, 2$;
11 **if** $\{\mathbf{x}_k^{(l)}\}$ *satisfies the constraints of* (21b), (21c), *and* (21d), *and* $d_i \leq \xi_i (i = 1, 2)$ **then**
12 **if** $fc^{(l)} < fc^{(l^*)}$ **then** $l^* = l$;
13 **if** $|\frac{fc^{(l)} - fc^{(l-1)}}{fc^{(l-1)}}| \leq \delta$ **then break** ;
14 **end**
15 **end**
16 Set $\{\mathbf{u}^*(k) = \mathbf{u}_k^{(l^*)}, \mathbf{x}^*(k) = \mathbf{x}_k^{(l^*)}\}$ and $fc^* = fc^{(l^*)}$;

$N-1\}$. To alleviate the dependency, this paper uses quasilinearization method to iteratively find the best solution [26], [35], [40]. The principle is to iteratively linearize the nonlinear state update equations and the constraints and find the corresponding QP solutions. The optimal control sequence obtained at one iteration is used as the estimated control sequence for the next iteration. The initial estimate is obtained from a non-predictive simple controller and the iterations continue until a convergence criterion is satisfied or a maximal iteration limit is reached.

Algorithm 1 shows the quasilinearization method. For simplicity, the range of the time step k is ignored in Algorithm 1, because the ranges of the control inputs and state vectors are always $k = 0, \ldots, N-1$ and $k = 0, \ldots, N$, respectively. The superscript l enclosed by parentheses indicates values obtained at the lth iteration. Variable l^* indicates the optimal solution satisfying all state constraints and achieving the smallest fuel consumption. Parameter $maxIter$ at line 5 is a positive integer to limit the maximal number of iterations. The sequence $\{\overline{\mathbf{x}}_k^{(l)}\}$ at line 7 is the state sequence estimated by the linear approximation model in (32) and is obtained together with $\{\mathbf{u}_k^{(l)}\}$ through solving the QP problem. Line 10 computes the RMSE of the two states between the nonlinear model and the linear model with the same control sequence. The QP solution is accurate only if the RMSE of the two states are less than the tolerances ξ_i $(i = 1, 2)$. Parameter δ at line 13 is a small number indicating the convergence of the quasilinearization algorithm.

Theorem 1: Algorithm 1 terminates within $maxIter$ iterations. If the state sequence $\{\mathbf{x}_k^{(0)}\}$ obtained by the initial estimate of the control sequence $\{\hat{\mathbf{u}}_k\}$ satisfies all constraints of (21b), (21c), and (21d), the output of the optimal state sequence $\{\mathbf{x}^*(k)\}$ must also satisfy all these constraints and $fc^* \leq fc^{(0)}$.

Proof: Since the for-loop at line 5 specifies an iteration upper bound, the algorithm must terminate with at most $maxIter$ iterations.

At line 1, l^* is initiated as 0. When the algorithm terminates, two cases may occur: $l^* = 0$ or $l^* > 0$. If $l^* = 0$, then $\mathbf{x}^*(k) = \mathbf{x}_k^{(0)}$ for $k = 0, \ldots, N$ and $fc^* = fc^{(0)}$. The statements in the theorem hold trivially. If $l^* > 0$ at line 16, the assignment $l^* = l$ $(l > 0)$ at line 12 must be executed. The necessary condition to execute the assignment operation is the sequence $\{x_k^{(l)} | k = 0, \ldots, N\}$ satisfies constraints (21b), (21c), and (21d) and $fc^{(l)} < fc^{(0)}$. ■

The maximal coolant temperature limit in (21c) is most critical. Owing to the modeling error of the linear time-varying coolant temperature model, even though the QP solution satisfies the constraint, the maximal coolant temperature of the nonlinear model may still exceed the upper bound. To avoid the violation, we compensate the modeling error in the constraint in (21c). At iteration $l > 1$, the error between the nonlinear coolant model and the linear model at the last iteration $l-1$ is computed as follows.

$$err_k^{(l-1)} = \max\left(0, T_{e\_k}^{(l-1)} - \overline{T}_{e\_k}^{(l-1)}\right), k = 0, \ldots, N$$

At line 6 of Algorithm 1, the constraint on the coolant temperature is updated to

$$T_{e\_min} \leq T_e(k) \leq T_{e\_max} - err_k^{(l-1)}$$

V. Numerical Comparison

A conventional truck VOLVO FH 460HP 6 × 2 Tractor with the electric cooling system is studied in this paper. Its maximal gross weight is 60 tonnes and emission level EURO 6. The engine is 13 liter with the maximal power 460 hp at 1400–1800 rpm and the maximal torque 2300 Nm at 1400 rpm. The same truck is employed in [8], [9], [13], [14]. The accuracy of the cooling system model in (1) is verified in [9] and the normalized RMSE is less than 3%. In the following simulation studies, the weights of the simulated truck are 40 or 60 tonnes, and the ambient temperature is 35 °C.

A. Drive Cycles

Two drive cycles are chosen for simulation. One is a real route of around 90 km recording a round trip between Borås and Landvetter in Sweden. The route is called BLB. The other is an extension of the standard drive cycle ACEA Long Haul published by the European Association of Car Manufacturers (ACEA) [41]. The route is designed for long haul trucks for goods deliveries and consists of mainly highway operations and

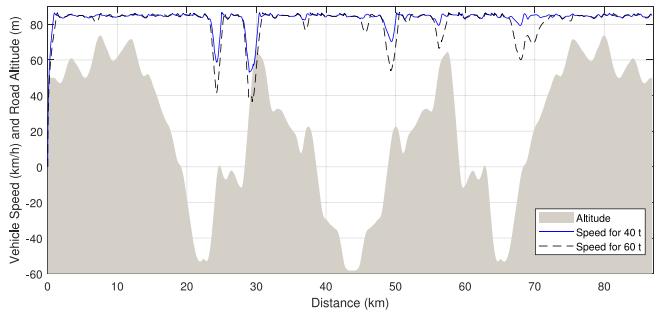

(a)

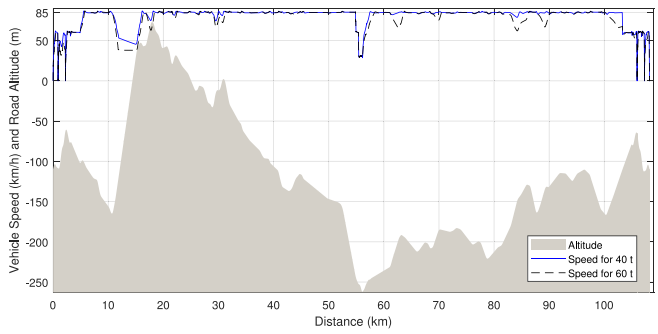

(b)

Fig. 2. The Drive Cycles. (a) The BLB Cycle. (b) The ACEA Long Haul Cycle.

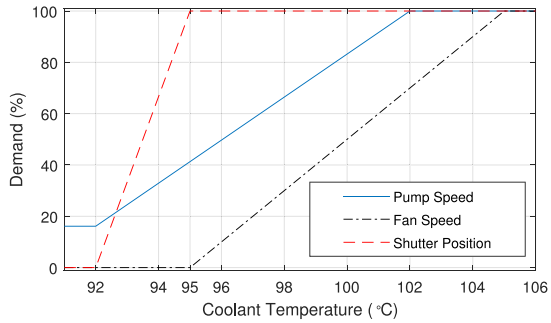

Fig. 3. The Baseline Controller.

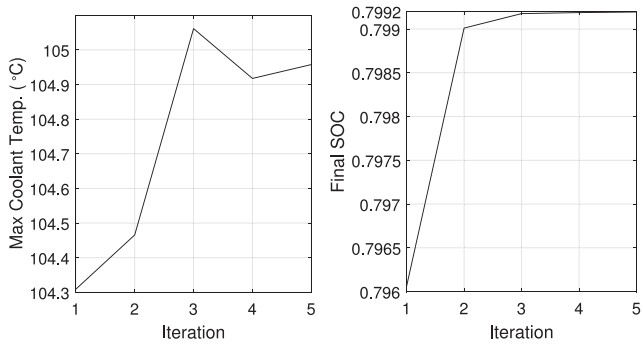

(a) (b)

Fig. 4. State Constraints of Algorithm 1. (a) Maximal Coolant Temperature. (b) Final SOC.

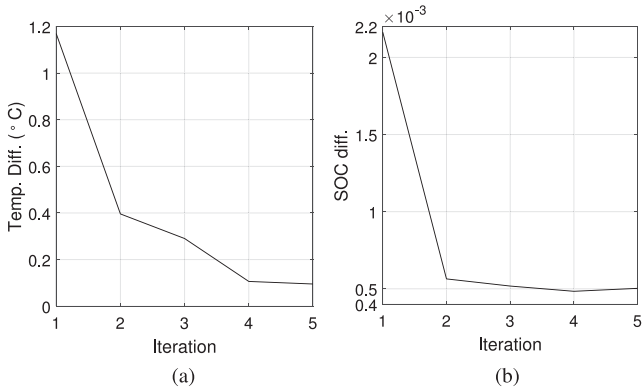

(a) (b)

Fig. 5. Differences between the Linear and the Nonlinear Models. (a) RMSE of Coolant Temperature. (b) RMSE of SOC.

a small part of regional roads. Its length is around 110 km. The speed trajectories and road altitude profiles of the two cycles are illustrated in Fig 2. The height differences of the two roads are around 130 and 310 m, respectively. The traveling times of the 40 and 60 tonne trucks on the BLB cycle are 3772 and 3922 seconds, respectively. The traveling times of the 40 and 60 tonne trucks on the ACEA cycle are 5388 and 5636 seconds, respectively.

B. Convergence of the Quasilinearization Method

This section verifies the convergence property of the quasilinearization algorithm in Algorithm 1. The algorithm starts with an initial estimate of the control sequence, which is determined by a baseline controller in this paper. The baseline controller simply determines the speeds of the coolant pump and the radiator fans and the shutter position by coolant temperature according to three 1D lookup tables illustrated in Fig. 3. The battery current is constant 0 A.

The plots show the percentages of the control demands. The maximal speeds of the pump and the fans are 3100 and 3400 rpm, respectively. The minimal pump speed is 500 rpm (16.13%). The thermostat is closed when the coolant temperature is below 82 °C and fully open when the temperature becomes 92 °C. Afterward, when the coolant temperature rises, the pump speed increases and reaches the maximal speed at 102 °C. The shutter is closed when the coolant temperature is less than 92 °C and becomes fully open when the coolant temperature reaches 95 °C. After the shutter is fully open, the fans speed starts to increase when the coolant temperature is larger than 95 °C and reaches its maximum at 105 °C.

This section elaborates the converging process of Algorithm 1 for a 40 tonne truck on the BLB cycle. The time step is $\Delta t = 2$ seconds. Then the total number of sampling steps is $N = 1886$. According to (34), the number of optimization variables is $6\,N = 11316$. Let $maxIter = 5$ in Algorithm 1. Fig. 4(a) visualizes that the maximal coolant temperature is safe in all iterations except the third one. Fig. 4(b) shows that the final SOC converges to acceptable values from the second iteration. The plots in Fig. 5 show the RMSE of coolant temperature and SOC between the linear and the nonlinear models. The differences

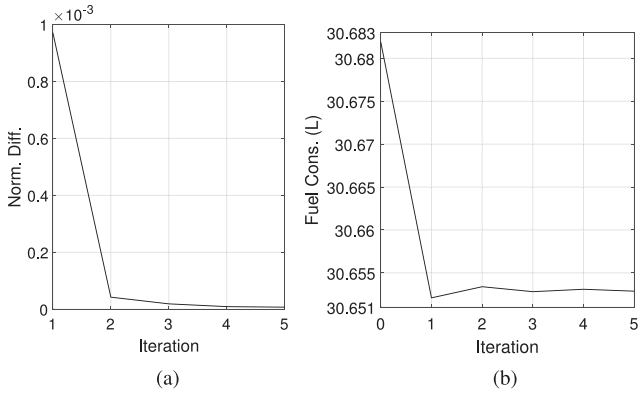

Fig. 6. Termination Criterion and Fuel Consumption. (a) Termination Criterion. (b) Fuel Consumption.

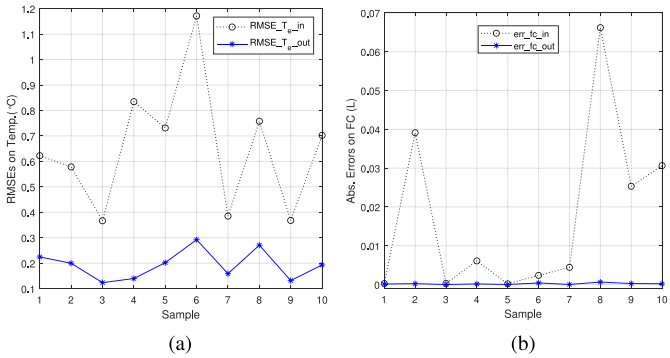

Fig. 7. Sensitivity Analysis of Random Initial Control Sequences. (a) RMSE of T_e.(b) Absolute errors of fc.

between the two models quickly decrease to acceptable small values.

The termination criterion of Algorithm 1, as in line 13, is the normalized difference between the fuel consumptions of two consecutive iterations. The values of five iterations are plotted in Fig. 6(a). The fuel consumptions of the truck during the iterations of Algorithm 1 are plotted in Fig. 6(b). Compared with other plots in this subsection, the iteration axis starts at 0, which indicates the fuel consumption by the baseline controller shown in Fig. 3. The fuel consumptions of iterations 1-5 are obtained by the QP method presented in Section IV. Fig. 6 shows that both termination criterion and fuel consumption converge after 3 iterations.

The outcome of Algorithm 1 is dependent on several tuning parameters. If at line 11 the maximal difference between the final SOC and the initial SOC is 0.001, the maximal coolant temperature is 105 °C, the maximal RMSE of the coolant temperature and the SOC are $\xi_1 = 0.2$ °C and $\xi_2 = 0.001$, and termination threshold at line 13 is $\delta = 10^{-4}$, then Algorithm 1 terminates after 4 iterations and the minimal fuel consumption at this case is 30.653 liters. Although Fig. 6(b) shows that the fuel consumption at iteration 1 is minimal, Fig. 4(b) shows the final SOC at iteration 1 violates the constraint.

Similar converging properties are observable for all other test cases: 40/60 tonne trucks on the BLB/ACEA cycles. There are all together four test cases. Owing to space limit, plots of the other three cases are skipped.

C. Robustness of the Quasilinearization Method

This section shows the robustness of Algorithm 1 against random initial control estimates via Monte Carlo simulations. The result also implies that the iterative QP method can find the real optimum of the nonlinear optimization problem (21a). Random perturbations are added to the baseline controller in Fig. 3 to generate distinct initial control sequences. The control demand to each of the three actuators is characterized by two switching temperature values. For example, the first switching temperature of the pump is 92 °C and the second is 102 °C. The six switching values in Fig. 3 are replaced by six random variables with the uniform distribution. The ranges of the two switching values of the pump are 92 ± 4 and 102 ± 4. The ranges of the two switching values of the fans are 95 ± 4 and 105 ± 4. The ranges of the two switching values of the shutter are 92 ± 3 and 97.5 ± 2.5.

Every iteration of the Monte Carlo simulation generates a random sample of the six switching value. The sample then determines a perturbed baseline controller, which generates a control sequence $\{\hat{\mathbf{u}}_k | k = 0, \ldots, N-1\}$, the corresponding state sequence $\{\hat{\mathbf{x}}_k | k = 0, \ldots, N\}$, and the fuel consumption $fc^{(0)}$. To quantify the influence of the randomly perturbed baseline controller, we calculate the RMSE of the estimated temperature sequences obtained by the normal and the randomly perturbed baseline controllers, and the absolute difference of the fuel consumptions $fc^{(0)}$ between the two baseline controllers. Denote the two error values as $RMSE\_T_e\_in$ and err_fc_in. Algorithm 1 takes the control sequence as the input and then returns the optimal control and state sequences $\{\mathbf{u}_k^* | k = 0, \ldots, N-1\}$, $\{\mathbf{x}_k^* | k = 0, \ldots, N\}$ and the minimal fuel consumption fc^*. We also calculate the RMSE of the optimal temperature sequences obtained by the normal and the randomly perturbed baseline controllers, and the absolute difference of the optimal fuel consumptions achieved by the normal and perturbed baseline controllers. Denote the two error values as $RMSE\_T_e\_out$ and err_fc_out.

Fig. 7(a) shows the comparison between $RMSE\_T_e\_in$ and $RMSE\_T_e\_out$ for 10 random samples for the 40 tonne truck on the BLB cycle. Fig. 7(b) shows the comparison between err_fc_in and err_fc_out for the same 10 samples. The means and standard deviations of $RMSE\_T_e\_in$ and $RMSE\_T_e\_out$ are (0.652, 0.25) and (0.194, 0.057), respectively. The means and standard deviations of err_fc_in and err_fc_out are $(1.75, 2.23) \times 10^{-2}$ and $(2.16, 1.96) \times 10^{-4}$, respectively. Despite large deviations on the inputs to Algorithm 1, its outputs have much less deviations. The result confirms the robustness of Algorithm 1.

D. Computation Time Measurement

The computations are implemented by MATLAB 2018b on a PC with Intel Core i7-4810MQ@2.80 GHz and 16 GB RAM.

TABLE I
COMPUTATION TIME OF ALGORITHM 1

Cases	Nbr. Var.	QP Time	Alg. Time	Nbr. Iter.
BLB 40T	$6 \times 1886 = 11316$	(2.475, 0.244)	(12.73, 0.857)	(4.09, 0.3)
BLB 60T	$6 \times 1961 = 11766$	(2.732, 0.262)	(14.894, 1.907)	(4.4, 0.5)
ACEA 40T	$6 \times 2694 = 16164$	(4.36, 0.352)	(24.22, 2.855)	(4.7, 0.5)
ACEA 60T	$6 \times 2818 = 16908$	(4.461, 0.389)	(26.6, 0.581)	(5, 0)

The time step for all cases is $\Delta t = 2$ s. The numbers of optimization variables for all test cases are listed in Table I. The computation times of both Algorithm 1 and the QP solution at Line 7 of the algorithm are measured during the Monte Carlo simulations in Section V-C. The mean values and standard deviations of the computation times in second and the number of iterations of Algorithm 1 are listed in Table I. The data in parentheses represent (Mean, Standard Deviation).

E. Fuel Efficiency and Thermal Management

This section compares fuel consumptions of the iterative QP (IQP) method, the baseline controller, and the dynamic programming (DP) method [35], [36]. The baseline controller represents a non-predictive and simple state feedback control emulating the state-of-practice of vehicular cooling system control. The baseline controller emphasizes the thermal safety of the engine rather than the energy consumption of the cooling system. The DP method represents another extreme on finding the global optimal solution that both ensures thermal safety and minimizes energy consumption. DP is preferred to PMP, because the result of DP contains lookup tables that can be used as optimal state-based feedback controllers when the actual state value is different from the offline optimal state trajectory. A fundamental difference between the DP and the QP methods is that the DP method uses the original nonlinear model of the cooling system without any simplification.

Table II lists the fuel consumptions and average coolant temperatures of the three comparison controllers for all test cases. For all comparison items, the baseline controller always has the largest fuel consumptions. The rows on reduced consumptions compute the relative difference in percentage between the iterative QP or the DP method and the baseline controller. For example, let m_{f_base} and m_{f_qp} be the total fuel consumptions of the baseline controller and the iterative QP method, respectively. Then, the reduction on the total fuel consumption (Reduc. Total FC) of the three-input method is calculated as follows: $\frac{m_{f\_base} - m_{f\_qp}}{m_{f\_base}} \times 100\%$.

The first observation is that the iterative QP and the DP methods achieve very similar fuel consumptions, although the two methods employ completely distinct optimization approaches. The similarity confirms the correctness of the iterative QP method. Compared to the baseline controller, the two optimal controllers achieve around 0.5% reduction on the total fuel consumptions. The value seems marginal, but the optimal controllers mainly manage the cooling system, whose contribution to the fuel consumption is only around 1% for the baseline controller. If we compare only the auxiliary fuel consumptions of the alternator, the two optimal controllers achieve reductions from 33% to 59%. By contrast, the optimal controllers reduce only around 0.02% fuel consumptions of the driveline via the optimal control of the active shutter. The benefit of the active shutter is hence more on maintaining higher coolant temperature.

TABLE II
COMPARISON OF FUEL CONSUMPTIONS AND TEMPERATURES

Cases	Results	IQP	DP	Baseline
BLB 40T	Total FC (L)	30.66	30.657	30.781
	Reduc. Total FC	0.391%	0.40%	
	Driveline FC (L)	30.428	30.428	30.436
	Reduc. Drv. FC	0.025%	0.026%	
	Alternator FC (L)	0.232	0.229	0.344
	Reduc. Alt. FC	32.666%	33.48%	
	Avg. Temp. (°C)	93.95	92.18	90.31
BLB 60T	Total FC (L)	40.225	40.227	40.408
	Reduc. Total FC	0.454%	0.448%	
	Driveline FC (L)	40.017	40.02	40.026
	Reduc. Drv. FC	0.023%	0.016%	
	Alternator FC (L)	0.207	0.207	0.382
	Reduc. Alt. FC	45.711%	45.773%	
	Avg. Temp. (°C)	95.41	93.11	91.20
ACEA 40T	Total FC (L)	40.543	40.528	40.778
	Reduc. Total FC	0.577%	0.614%	
	Driveline FC (L)	40.274	40.274	40.282
	Reduc. Drv. FC	0.020%	0.021%	
	Alternator FC (L)	0.269	0.254	0.496
	Reduc. Alt. FC	45.809%	48.853%	
	Avg. Temp. (°C)	93.5	92.19	90.65
ACEA 60T	Total FC (L)	53.445	53.441	53.819
	Reduc. Total FC	0.695%	0.703%	
	Driveline FC (L)	53.188	53.188	53.198
	Reduc. Drv. FC	0.018%	0.019%	
	Alternator FC (L)	0.257	0.253	0.621
	Reduc. Alt. FC	58.601%	59.277%	
	Avg. Temp. (°C)	94.94	93.57	91.54

The plots in Figs. 8–12 illustrate the trajectories of states and control signals of the three comparison controllers for the 60 tonne truck on the ACEA cycle. The temperature trajectories of the two optimal controllers are very similar in Fig. 8(a). The optimal controllers use the coolant temperature as an energy buffer. Before the engine produces high power, e.g., at sections 10–18 km, 55–65 km, and 100–105 km, both optimal controllers decrease the coolant temperature to the minimum in advance. During the heavy load sections, the optimal controllers allow the coolant temperature to reach its maximum to reduce the auxiliary consumption of the cooling system. By contrast, the baseline controller does not exploit the coolant temperature as an energy buffer but tries to regulate the temperature around 91 °C regardless of the engine load.

The plots in Fig. 8(b) show the battery SOC of the three controllers. Since the baseline controller does not use battery electricity to drive the cooling system, the SOC of the baseline controller is constantly 0.8. The SOC trajectories of the two optimal controllers have noticeable difference, but both terminate at values close to the initial value of 0.8.

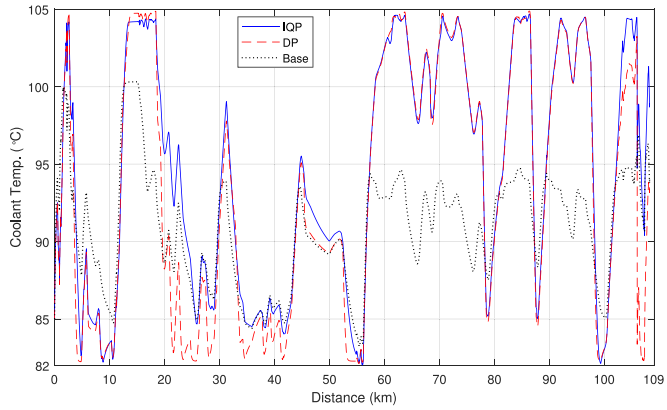

(a)

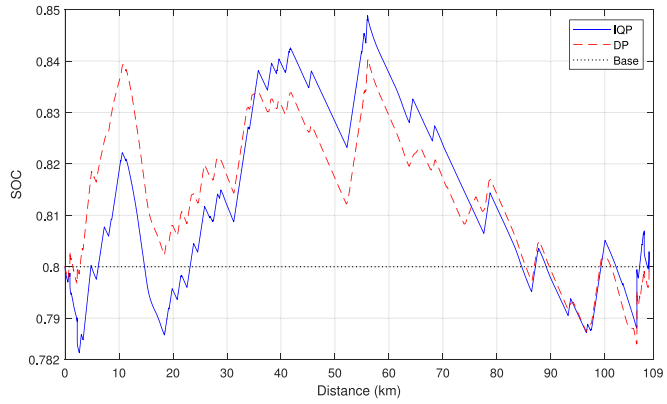

(b)

Fig. 8. State Trajectories of Three Controllers for a 60 T Truck on ACEA. (a) Coolant Temperature.(b) Battery SOC.

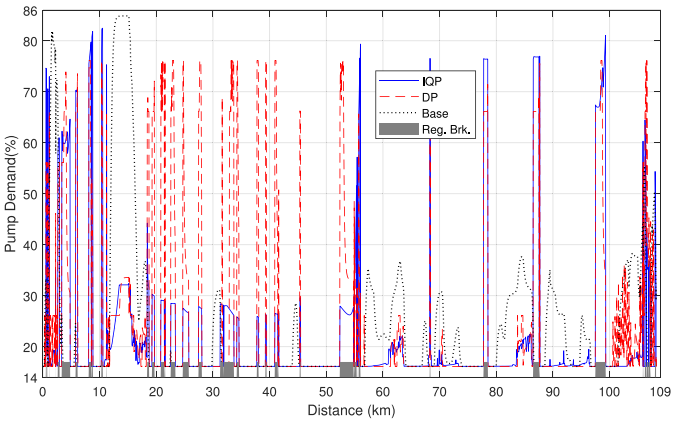

Fig. 9. Pump Speed Demands of The Three Controllers.

Figs. 9 and 10 compare the speed demands of the pump and the fans by the three controllers. Both the optimal controllers demand minimal speeds from the pump and the fans when the regenerative brake is not applied, except at the sections 10–20 km and 100–105 km. According to the drive cycle data in Fig. 2, the two sections are steep and long uphills. The engine produces a lot of heat while running the sections and large cooling effort is required to keep the coolant temperature safe, even though

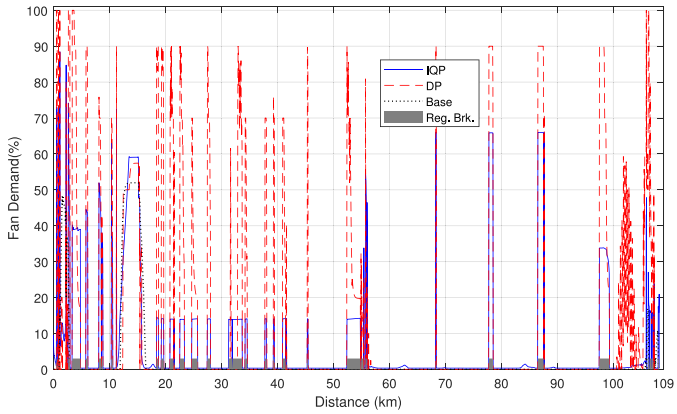

Fig. 10. Fan Speed Demands of The Three Controllers.

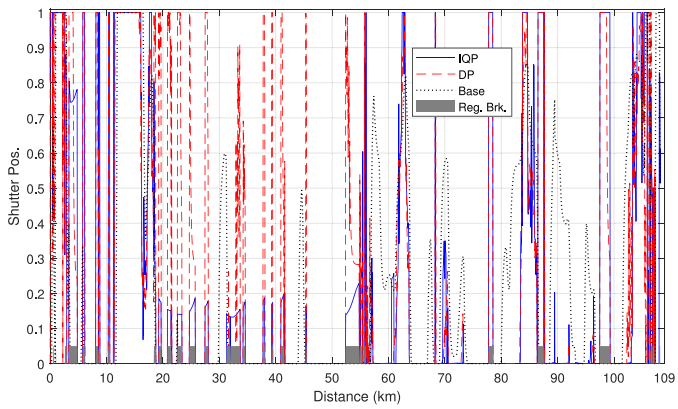

Fig. 11. Shutter Positions of The Three Controllers.

the optimal controllers have proactively decreased the coolant temperature to the minimum before the uphill.

When the regenerative brake is applied during 0 to 60 km, the DP controller demands larger speeds from the pump and the fans than the IQP controller does. The coolant temperature under the DP controller, therefore, is generally lower than that under the QP controller, as illustrated in Fig. 8(a). The baseline controller does not take advantage of the regenerative brake and often requires larger pump speed than the two optimal controllers do when the regenerative brake is not applied. This increases the alternator fuel consumption. If the engine is already fully loaded by the driveline torque, the large pump speed creates large alternator torque and the total engine torque demand may be higher than its maximum. The two optimal controllers never violate the engine torque limit.

Fig. 11 compares the shutter position requests by the three controllers. The baseline controller generally demands larger shutter position when the regenerative brake is not applied. This is a reason that the baseline controller achieves slightly larger driveline fuel consumption. Fig. 12 compares the battery current trajectories determined by the three controllers. As discussed before, the baseline controller does not use the battery electricity. When the regenerative brake is applied, both optimal controllers always demand the maximal charging current to recharge the battery by the free energy. When the brake is not applied, the two optimal controllers generally take around 40 A from the battery

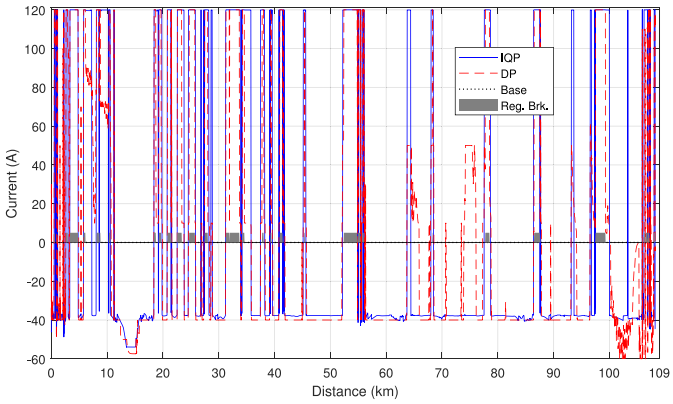

Fig. 12. Battery Currents of The Three Controllers.

TABLE III
BENEFITS OF THE RADIATOR SHUTTER

Cases	Results	Shutter	No Shutter	Diff.
BLB 40T	Total FC (L)	30.66	30.737	-0.248%
	Driveline FC (L)	30.428	30.505	-0.251%
	Alternator FC (L)	0.232	0.232	0.099%
	Mean&Std T_e	(93.95, 5.9)	(85.88, 2.13)	8.07
BLB 60T	Total FC (L)	40.225	40.29	-0.161%
	Driveline FC (L)	40.017	40.083	-0.164%
	Alternator FC (L)	0.207	0.207	0.37%
	Mean&Std T_e	(95.41, 6.82)	(87.39, 3.57)	8.02
ACEA 40T	Total FC (L)	40.543	40.624	-0.199%
	Driveline FC (L)	40.274	40.358	-0.206%
	Alternator FC (L)	0.269	0.266	0.935%
	Mean&Std T_e	(93.5, 6.55)	(87.6, 4.64)	5.9
ACEA 60T	Total FC (L)	53.445	53.515	-0.131%
	Driveline FC (L)	53.188	53.260	-0.136%
	Alternator FC (L)	0.257	0.255	0.795%
	Mean&Std T_e	(94.94, 7.41)	(89.46, 6.15)	5.48

to drive the electric cooling system. At the two steep uphills at 10–20 km and 100–105 km, the optimal controllers request large current from the battery to drive the electric cooling systems. The electrical energy from the battery greatly reduces the alternator fuel consumption during the heavy load sections.

F. Benefits of the Active Shutter

This section presents the benefits of the active grille shutter for the fuel consumptions and thermal management of automotive engine cooling systems through comparing the results of the iterative QP controller for the same electric cooling system with and without the active shutter. The latter controller is equivalent to the iterative QP controller if the shutter position is fixed to constant 1. Table III presents the comparison results. The rows labeled by "Mean&Std" show the mean and standard deviation of the coolant temperature and shutter position, respectively. The column labeled by "Diff." shows the difference between the values with and without the shutter. If the difference is the relative value in percentage, the denominator is the value without the shutter. The differences of coolant temperature and shutter position are only for the mean values.

Table III shows that the active shutter can slightly decrease the total fuel consumption, because of the decreased aerodynamic drag. The table shows positive causal relationship between the reduction of the average shutter position and the reductions on both total and driveline fuel consumptions. The negative impact of the shutter is the increase of alternator fuel consumption, because the closed shutter decreases the radiator air flow and the coolant temperature becomes higher. The shutter increases the average coolant temperature but the corresponding controller still keeps the temperature within the safe limits. Higher coolant temperature may increase combustion efficiency, reduce friction of the lubricant oil, and increase the efficiency of exhaust catalysts [15], [27]. The radiator shutter hence has the benefits of increasing engine energy efficiency and decreasing pollutant emissions.

VI. CONCLUSION AND FUTURE WORK

The paper applies iterative quadratic programming and quasi-linearization methods to the optimal control of the automotive electric engine cooling system with the active grille shutter. The coolant and the battery are exploited as energy buffers for improving engine efficiency and recuperating brake energy. The original formulation of the energy minimization problem is a complicated nonlinear optimization problem with nonlinear cost and constraints. Its direct solution is time consuming. A main contribution of this paper is to approximate it by a convex quadratic problem with linear constraints, which can be solved efficiently in large scale. To mitigate the discrepancy between the approximate and original models, the quasilinearization method is adopted to iteratively find approximations of the original models and solve QP problems until the answers are sufficiently accurate.

Compared with a rule-based baseline controller, the proposed optimal control method reduces the total fuel consumption by 0.39% to 0.69% and the alternator fuel consumption by 32.67% to 58.6%. The active grille shutter reduces the total fuel consumption by 0.13% to 0.25% and increases the average coolant temperature by 5.5 °C to 8.1 °C.

This paper is limited to the global optimal control for the complete drive cycle, but the same method can be adapted to MPC, where the drive cycle data within a limited prediction horizon are estimated online [9]. We shall develop the real-time MPC controller and test it on a high-fidelity simulation model or an experimental truck in the future. The influences of higher coolant temperature on fuel efficiency and exhaust emission will also be studied.

REFERENCES

[1] A. Lajunen, Y. Yang, and A. Emadi, "Recent developments in thermal management of electrified powertrains," *IEEE Trans. Veh. Technol.*, vol. 67, no. 12, pp. 11486–11499, Dec. 2018.

[2] M. H. Salah, T. H. Mitchell, J. R. Wagner, and D. M. Dawson, "Nonlinear-control strategy for advanced vehicle thermal-management systems," *IEEE Trans. Veh. Technol.*, vol. 57, no. 1, pp. 127–137, Jan. 2008.

[3] P. Setlur, J. Wagner, D. Dawson, and E. Marotta, "An advanced engine thermal management system: Nonlinear control and test," *IEEE/ASME Trans. Mechatronics*, vol. 10, no. 2, pp. 210–220, Apr. 2005.

[4] M. H. Salah, T. H. Mitchell, J. R. Wagner, and D. M. Dawson, "A smart multiple-loop automotive cooling system-model, control, and experimental study," *IEEE/ASME Trans. Mechatronics*, vol. 15, no. 1, pp. 117–124, Feb. 2010.

[5] T. Wang and J. Wagner, "Advanced engine cooling system subject to Ram air effect-nonlinear adaptive multiple input and multiple output (NAMIMO) control," *IEEE Trans. Veh. Technol.*, vol. 66, no. 9, pp. 7730–7740, Sep. 2017.
[6] M. Nilsson, L. Johannesson, and M. Askerdal, "Assessing the potential of prediction in energy management for ancillaries in heavy-duty trucks," in *Proc. Eur. Control Conf.*, Strasbourg, France, Jun. 2014, pp. 1693–1698.
[7] N. Pettersson and K. H. Johansson, "Modelling and control of auxiliary loads in heavy vehicles," *Int. J. Control*, vol. 79, no. 5, pp. 479–495, 2006.
[8] M. Khodabakhshian, L. Feng, and J. Wikander, "Predictive control of the engine cooling system for fuel efficiency improvement," in *Proc. IEEE Int. Conf. Autom. Sci. Eng.*, Taipei, Taiwan, 2014, pp. 61–66.
[9] M. Khodabakhshian, L. Feng, S. Börjesson, O. Lindgärde, and J. Wikander, "Reducing auxiliary energy consumption of heavy trucks by onboard prediction and real-time optimization," *Appl. Energy*, vol. 188, pp. 652–671, 2016.
[10] C. Pfeifer, "Evolution of active grille shutters," SAE Technical Paper, Tech. Rep. 2014-01-0633, Detroit, Michigan, USA, Apr. 2014.
[11] S. Baskar and R. Rajaraman, "Airflow management in automotive engine cooling system—Overview," *Int. J. Thermal Technol.*, vol. 5, no. 1, pp. 1–8, 2015.
[12] T. Kubokura, T. Uno, N. Evans, H. Kuroda, F. Shindo, and S. Nagahama, "Study of cooling drag reduction method by controlling cooling flow," SAE Technical Paper, Tech. Rep. 2014-01-0679, Detroit, Michigan, USA, Apr. 2014.
[13] O. Lindgärde, L. Feng, A. Tenstam, and M. Söderman, "Optimal vehicle control for fuel efficiency," *SAE Int. J. Commercial Vehicles*, vol. 8, no. 2, pp. 682–694, 2015.
[14] O. Lindgärde, M. Söderman, A. Tenstam, and L. Feng, "Optimal complete vehicle control for fuel efficiency," *Transp. Res. Procedia*, vol. 14, pp. 1087–1096, 2016.
[15] A. Roberts, R. Brooks, and P. Shipway, "Internal combustion engine cold-start efficiency: A review of the problems, causes, and potential solutions," *Energy Convers. Manag.*, vol. 82, pp. 327–350, 2014.
[16] A. Y. Karnik, A. Fuxman, P. Bonkoski, M. Jankovic, and J. Pekar, "Vehicle powertrain thermal management system using model predictive control," *SAE Int. J. Mater. Manuf.*, vol. 9, no. 3, pp. 525–533, 2016.
[17] P. Bonkoski, A. Y. Karnik, and A. Fuxman, "Calibration and demonstration of vehicle powertrain thermal management using model predictive control," *SAE Int. J. Engines*, vol. 10, no. 2, pp. 173–180, 2017.
[18] Y.-C. Cho, C.-W. Chang, A. Shestopalov, and E. Tate, "Optimization of active grille shutters operation for improved fuel economy," *SAE Int. J. Passenger Cars-Mech. Syst.*, vol. 10, no. 2, pp. 563–572, 2017.
[19] J. Bouilly, F. Lafossas, A. Mohammadi, and R. Van Wissen, "Evaluation of fuel economy potential of an active grille shutter by the means of model based development including vehicle heat management," *SAE Int. J. Engines*, vol. 8, no. 5, pp. 2394–2401, 2015.
[20] R. Mustafa, M. Schulze, P. Eilts, F. Küçükay, T. Jaeckel, and C. Lund, "Improved energy management using engine compartment encapsulation and grille shutter control," *SAE Int. J. Fuels Lubricants*, vol. 5, no. 2, pp. 803–812, 2012.
[21] J. Batteh, J. Gohl, and S. Chandrasekar, "Integrated vehicle thermal management in Modelica: Overview and applications," in *Proc. 10th Int. Modelica Conf.*, Lund, Sweden, Mar. 2014, pp. 409–418.
[22] K. Wang, C. Greiner, J. Batteh, and L. Li, "Integration of complex Modelica-based physics models and discrete-time control systems: Approaches and observations of numerical performance," in *Proc. 12th Int. Modelica Conf.*, Prague, Czech Republic, May 2017, pp. 527–532.
[23] V. Shigarkanthi, V. Damodaran, D. Soundararaju, and K. Kanniah, "Application of design of experiments and physics based approach in the development of aero shutter control algorithm," SAE Technical Paper, Tech. Rep. 2011-01-0155, Detroit, Michigan, USA, Apr. 2011.
[24] A. Nguyen, J. Lauber, and M. Dambrine, "Optimal control based algorithms for energy management of automotive power systems with battery/supercapacitor storage devices," *Energy Convers. Manag.*, vol. 87, pp. 410–420, 2014.
[25] J. A. Petersen and M. Bodson, "Constrained quadratic programming techniques for control allocation," *IEEE Trans. Control Syst. Technol.*, vol. 14, no. 1, pp. 91–98, Jan. 2006.
[26] M. Li and H. Peng, "Solutions of nonlinear constrained optimal control problems using quasilinearization and variational pseudospectral methods," *ISA Trans.*, vol. 62, pp. 177–192, 2016.
[27] A. K. Haghighat, S. Roumi, N. Madani, D. Bahmanpour, and M. G. Olsen, "An intelligent cooling system and control model for improved engine thermal management," *Appl. Thermal Eng.*, vol. 128, pp. 253–263, 2018.
[28] X. Zhang, Z. Wu, X. Hu, W. Qian, and Z. Li, "Trajectory optimization-based auxiliary power unit control strategy for an extended range electric vehicle," *IEEE Trans. Veh. Technol.*, vol. 66, no. 12, pp. 10 866–10 874, Dec. 2017.
[29] F. Willems, F. Kupper, and R. Cloudt, "Integrated powertrain control for optimal CO_2-NO_x tradeoff in an Euro-VI diesel engine with waste heat recovery systems," in *Proc. Amer. Control Conf.*, Montreal, Canda, Jul. 2012, pp. 1296–1301.
[30] J. Kessels, F. Willems, W. Schoot, and P. van den Bosch, "Integrated energy and emission management for hybrid electric truck with SCR aftertreatment," in *Proc. IEEE Vehicle Power Propulsion Conf.*, Lille, France, Sept. 2010, pp. 1–6.
[31] M. Nilsson and L. Johannesson, "Convex optimization for auxiliary energy management in conventional vehicles," in *Proc. IEEE Vehicle Power Propulsion Conf.*, Coimbra, Portugal, Oct. 2014, pp. 1–6.
[32] C. Vermillion, J. Sun, and K. Butts, "Modeling, control design, and experimental validation of an overactuated thermal management system for engine dynamometer applications," *IEEE Trans. Control Syst. Technol.*, vol. 17, no. 3, pp. 540–551, May 2009.
[33] U. Kiencke and L. Nielsen, *Automotive Control Systems for Engine, Driveline, and Vehicle*, 2nd ed. Berlin Heidelberg, Germany: Springer-Verlag, 2005.
[34] L. Guzzella and A. Sciarretta, *Vehicle Propulsion Systems: Introduction to Modeling and Optimization*, 3rd ed. Berlin Heidelberg, Germany: Springer, 2013.
[35] D. E. Kirk, *Optimal Control Theory: An Introduction*. Mineola, New York, USA: Dover Publications, 2004.
[36] O. Sundström and L. Guzzella, "A generic dynamic programming MATLAB function," in *Proc. 18th IEEE Conf. Control Appl.*, Saint Petersburg, Russia, Jul. 2009, pp. 1625–1630.
[37] D. Fares, R. Chedid, F. Panik, S. Karaki, and R. Jabr, "Dynamic programming technique for optimizing fuel cell hybrid vehicles," *Int. J. Hydrogen Energy*, vol. 40, pp. 7777–7790, 2015.
[38] J. Liu, L. Feng, and Z. Li, "The optimal road grade design for minimizing ground vehicle energy consumption," *Energies*, vol. 10, no. 5, p. 700, 2017.
[39] A.-A. Mamun, Z. Liu, D. M. Rizzo, and S. Onori, "An integrated design and control optimization framework for hybrid military vehicle using lithium-ion battery and supercapacitor as energy storage devices," *IEEE Trans. Transp. Electrific.*, vol. 5, no. 1, pp. 239–251, Mar. 2019.
[40] H. Jaddu, "Direct solution of nonlinear optimal control problems using quasilinearization and chebyshev polynomials," *J. Franklin Inst.*, vol. 339, no. 4-5, pp. 479–498, 2002.
[41] V. Franco, O. Delgado, and R. Muncrief, "Heavy-duty vehicle fuel-efficiency simulation: A comparison of US and EU tools," ICCT (The International Council on Clean Transportation), Washington DC, USA, White Paper, 2015.

Lei Feng (Member, IEEE) received the B.S. and M.S. degrees from Xi'an Jiaotong University, Xi'an, China, in 1998 and 2001, respectively, and the Ph.D. degree from the Systems Control Group, the University of Toronto, Toronto, ON, Canada, in 2007. In 2012, he joined the Mechatronics and Embedded Control System Division, the KTH Royal Institute of Technology, Stockholm, Sweden, where he is currently an Associate Professor. His main research interests include energy management control of mechatronic systems, autonomous driving, verification and control synthesis of cyber-physical systems, and supervisory control of discrete-event systems.

Jan Wikander received the M.Sc. degree in mechanical engineering and the Ph.D. degree in mechatronics from the KTH Royal Institute of Technology, Stockholm, Sweden, in 1980 and 1988, respectively. After receiving the Ph.D. degree he has been deeply engaged in creating and building up a strong basis for research cooperation between KTH and the Swedish industry. This has led to the foundation of a group of industries involved with mechatronics research activities and the foundation of an Industrial Research Program on Mechatronics. In 1996, he was appointed as a Professor of mechatronics with KTH (the first full professorship to be established in Sweden) and in 1997, he was appointed as the Head of the Department of Machine Design. From 2013 to 2019, he was the Dean of School of Industrial Engineering and Management, KTH. His current research interests include mechatronics in general and especially control strategies and control system implementations for the control of complex mechanical systems.

Zhiwu Li (Fellow, IEEE) received the B.S. degree in mechanical engineering, the M.S. degree in automatic control, and the Ph.D. degree in manufacturing engineering from Xidian University, Xi'an, China, in 1989, 1992, and 1995, respectively. He joined Xidian University in 1992. He was a Visiting Professor with the University of Toronto, Toronto, ON, Canada, the Technion-Israel Institute of Technology, Haifa, Israel, the Martin-Luther University of Halle-Wittenburg, Halle, Germany, Conservatoire National des Arts et Métiers, Paris, France, and Meliksah Universitesi, Kayseri, Turkey. He is currently with the Institute of Systems Engineering, Macau University of Science and Technology, Macau, China. His current research interests include Petri net theory and applications, supervisory control of discrete-event systems, work-flow modeling and analysis, system reconfiguration, game theory, and data and process mining. Prof. Li chairs the Discrete-Event Systems Technical Committee of the IEEE Systems, Man, and Cybernetics Society and served as a member of IFAC Technical Committee on Discrete-Event and Hybrid Systems, from 2011 to 2014. He was the recipient of the Alexander von Humboldt Research Grant, Alexander von Humboldt Foundation, Germany. He is listed in *Marquis Whos Who in the World* (27th ed., 2010). He is the Founding Chair of Xian Chapter of IEEE Systems, Man, and Cybernetics Society. He serves as a frequent Reviewer for more than 90 international journals, including *Automatica*, a number of IEEE Transactions, and many international conferences.